Original papers

Med Ultrason 2025, Vol. 27, no. 4, 406-413
DOI: 10.11152/mu-4526

A nomogram based on clinical and ultrasound characteristics for predicting peripheral nerve schwannomas in soft tissue

Fan Yang, Yuan Chen, Huolin Wu, Jianmei Lei, Jingyuan Liu, Lingfang Yu, Jian Chen

Department of Ultrasound, The 907th Hospital of Chinese PLA Joint Logistics Support Force, Nanping, China

Abstract

Aims: To develop a nomogram that integrates clinical and ultrasound (US) characteristics for the preoperative prediction of peripheral nerve schwannomas in soft tissue. **Material and methods:** A retrospective analysis was conducted on 301 patients with soft tissue masses who underwent surgical excision and preoperative US evaluation. Clinical data and US features were collected and analyzed. Univariate and multivariate regression analyses were performed to identify independent predictors; subsequently, a nomogram was developed for predicting schwannomas. The performance of the nomogram was assessed using the area under the receiver operating characteristic curve (AUC), calibration curves, and decision curve analysis (DCA). Additionally, internal validation was performed using 10-fold cross-validation with 1000 iterations. **Results:** Seven independent predictors were identified, including target sign, rat tail sign, split fat sign, shape, layer, vascularity, and age. The nomogram demonstrated favorable discrimination and calibration, with an area under the receiver operating characteristic curve (AUC) of 0.934 (95% CI: 0.902–0.966). Furthermore, decision curve analysis (DCA) confirmed the nomogram's clinical utility across a wide range of risk thresholds (0.01–0.93). Internal validation yielded a corrected AUC of 0.921 (95% CI: 0.917–0.924). **Conclusion:** This nomogram provides clinicians with a quantitative and visual tool for preoperative prediction of schwannomas in soft tissue, thereby improving diagnostic accuracy and assisting in clinical decision-making.

Keywords: schwannoma; nomogram; ultrasonography; diagnosis; soft tissue neoplasms

Introduction

Schwannomas are the most frequent peripheral nerve sheath tumors, constituting 5% of all soft tissue neoplasms [1]. These tumors are encapsulated by the perineurium and predominantly consist of Schwann cells. They are commonly located on the flexor surfaces of the extremities, head and neck, and posterior spinal roots [2,3]. Most schwannomas are solitary and sporadic; however, multiple lesions can occur in the setting of neurofibromatosis type 2, often presenting as bilateral eighth nerve schwannomas. Less commonly, they are associated with schwannomatosis, which involves a somatic mutation of the NF2 gene [3,4].

Unlike the growth pattern of neurofibromas, schwannomas are typically well-encapsulated, compressing rather than infiltrating the nerve [5]. This characteristic enables complete resection of schwannomas without damaging the affected nerves [6]. Therefore, accurate preoperative diagnosis of schwannomas is essential for planning surgical procedures and preventing iatrogenic nerve injuries [7]. When schwannoma is suspected, preoperative biopsy is generally not recommended, as it significantly increases the risk of postoperative neurologic deficits [8]. Consequently, the preoperative diagnosis of schwannoma primarily relies on non-invasive imaging techniques, particularly ultrasound (US) and magnetic

Received 21.03.2025 Accepted 21.05.2025
Med Ultrason
2025, Vol. 27, No 4, 406-413
Corresponding author: Fan Yang
Department of Ultrasound,
The 907th Hospital of Chinese PLA
Joint Logistics Support Force,
99 Binjiangbei Road,
Nanping 353000, Fujian Province, China
Phone/fax: +86-0599-8849292
+86-0599-6987004
E-mail: yangf7811@163.com

resonance imaging (MRI) [9]. Recently, US has emerged as a portable, real-time imaging modality capable of identifying and guiding the treatment of multiple neurological complaints [10,11]. US offers several advantages, including low cost, ease of use, and high availability. It outperforms MRI in detecting small nerves and multiple lesions [12,13]. Additionally, US has no contraindications, whereas MRI is unsuitable for patients with cardiac pacemakers, metal implants, or claustrophobia. Therefore, US should be considered the preferred imaging modality for diagnosing peripheral nerve schwannomas [14,15].

Previous studies have reported that combining multiple US features significantly improves the accuracy of diagnosing schwannomas. This method aids in distinguishing schwannomas from other soft tissue tumors, such as angioleiomyomas [16,17]. We hypothesized that integrating clinical and US characteristics would lead to a more accurate assessment of schwannomas. However, to the best of our knowledge, no specific prediction model has been established for peripheral nerve schwannomas in soft tissue. The primary objective of this research is to develop a nomogram based on clinical and US characteristics, thereby facilitating the preoperative prediction of schwannomas and guiding clinical therapeutic regimens and surgical plans.

Material and methods

Patients

This study obtained approval from the institutional ethics review board, with a waiver of the informed consent requirement. A retrospective analysis was conducted on 716 consecutive patients with soft tissue masses in our hospital from June 2015 to June 2024. Inclusion criteria encompassed: (1) presence of a single mass; (2) underwent surgical excision; (3) received preoperative US evaluation within 2 weeks; (4) had comprehensive clinical and US documentation. Exclusion criteria comprised: (1) incomplete pathological records; (2) insufficient clinical data; (3) substandard US images or poor image quality. Ultimately, the study enrolled 301 patients meeting the aforementioned criteria, including 80 cases of schwannomas and 221 cases of non-schwannoma lesions. The flow chart of patient enrollment is shown in figure 1.

Clinical information

Two reviewers from the surgical department gathered clinical data of the enrolled patients from the medical records. One reviewer collected the data, and the other verified its accuracy. The collected clinical characteristics included demographic details such as gender and age, along with clinical manifestations, particularly focusing on the presence of neurological symptoms and signs. For instance, the presence of distal radiation numbness, pain, or anomalous sensations upon compression or traction of a mass indicates a positive Tinel's sign.

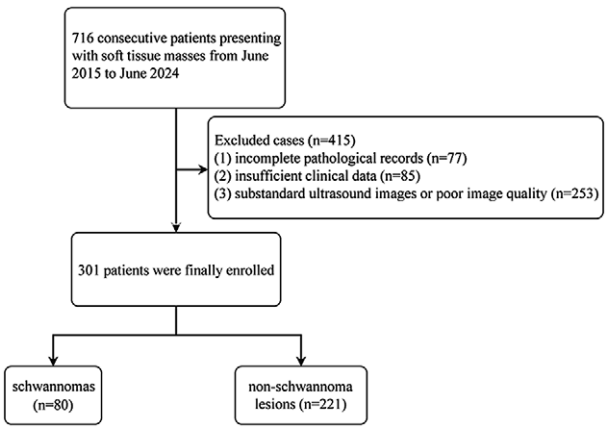

Fig 1. Flow chart of the patients enrolled in our study.

US image collection and feature interpretation

US examinations were conducted using an iU22 scanner (Philips Healthcare, Bothell, WA) equipped with a 5-12 MHz linear array transducer. The musculoskeletal US was executed in accordance with the instrument's preset protocol labeled "MSK Gen." The transducer frequency and focus were adjusted according to the structure of interest. The dynamic range was set between 56 and 66 dB; however, a reduced dynamic range was occasionally recommended to enhance the visualization of tumor heterogeneity. Additionally, Color Doppler US was performed with optimized parameters: the velocity scale was adjusted to 1.7-2.5 cm/s, the wall filter was set at 14-26 Hz, and the gain was optimized to minimize background noise.

The US images of all 301 patients were retrospectively analyzed by two radiologists (F.Y. and Y.C.), with 12 and 5 years of experience in musculoskeletal US, respectively. All images were independently reviewed using a local picture archiving and communication system (PACS) monitor. In cases of disagreement, they discussed the case together and reached a final consensus. Throughout the process, both radiologists remained blind to the patients' clinical information and pathological results.

Location, layer, dimensions, shape, margin, internal and posterior echoes of the mass, as well as its relationship with adjacent nerves, blood vessels, and surrounding tissues, and vascularity on color Doppler imaging were evaluated. The masses were categorized into three anatomical regions: head and neck, trunk, and limbs. Additionally, the tumors were classified as superficial if located in the dermal or subcutaneous fat layer, and classified

as deep if situated within the intermuscular or intramuscular regions. Measurements were taken for the longitudinal (L) and short (S) maximum diameter of the mass, and the L/S ratio was subsequently calculated. A mass was considered to have a regular shape when it presented as round, oval, or elliptical; otherwise, it was categorized as irregular. The margin of each mass was described as either well-defined or ill-defined. Anechoic areas within the mass indicated cystic components, while punctate or clustered markedly hyperechoic regions were identified as calcifications. The target sign was described as the presence of a cluster, cloud, or target-shaped hyperechoic area within the mass, with the peripheral region (more than 1 mm thick at its thickest point) of the mass being hypoechoic compared with the adjacent muscles [7]. The posterior echo of the mass was classified as enhanced or non-enhanced. The "rat tail sign" referred to the thin tail-shaped hypoechoic area extending from the nerve trunk, connected proximally or distally to one or both sides of the mass along its longitudinal axis. The "vessel accompanying sign" was considered positive when a mass was parallel and close to a vessel. The "split fat sign" was characterized by tapered hyperechoic regions adjacent to one or both ends of the mass's long axis [7]. The internal vascularity was semiquantitatively graded as previously described as follows: 0, no blood flow; I, minimal vascularity with the presence of one to two color dots or thin tumor vessels; II, moderate vascularity with the presence of three to four color dots or one penetrating vessel as long as or longer than the tumor's radius; and III, marked by vascularity with the presence of more than five color dots or two relatively long internal vessels [18]. Grades 0 to I were classified as hypovascular, while grades II to III were classified as hypervascular.

Statistical analysis

Statistical analyses were conducted using IBM SPSS Statistics for Windows, version 26.0 (IBM Corp., Armonk, NY, USA) and R software version 4.3.1 (The R Foundation for Statistical Computing, Vienna, Austria). Categorical variables were described as frequencies with corresponding percentages and assessed using Pearson's chi-square test. Continuous variables were presented as either mean ± standard deviation or as median and interquartile range, contingent upon the normality of the distribution. Comparative analysis of continuous variables was executed employing either the independent samples t-test or the Mann-Whitney U test, based on the data distribution. Univariate analyses were performed to identify potential influencing factors. Variables exhibiting a p-value < 0.05 were subsequently included in the multivariate logistic regression analysis for independent predictor selection, using the forward stepwise selection method. A nomogram derived from the multivariate analysis was utilized for schwannomas prediction. The nomogram's performance was assessed via the area under the receiver operating characteristic curve (AUC), calibration curves, and decision curve analysis (DCA). Internal validation of the model was performed using 10-fold cross-validation with 1000 iterations. Statistical significance was defined as a two-sided p-value <0.05.

Results

Pathological results

In the study, 301 patients presented with a total of 301 soft tissue masses. Among these, 80 were pathologically confirmed as benign schwannomas, while 221 were categorized as non-schwannoma cases, comprising 207 benign lesions and 14 malignant lesions. The histological types and composition of non-schwannoma lesions are listed in Table I.

Clinical and US characteristics

The clinical and US characteristics of patients with schwannomas and non-schwannoma lesions are presented in Table II. In univariate analysis, significant differences were found between schwannomas and non-schwannoma lesions in 14 out of the 18 variables ($p<0.05$), excluding gender, location, cystic component, and longitudinal maximum diameter (LMD).

Development of the nomogram

Multivariate logistic regression analysis identified 7 independent factors for predicting schwannomas, including target sign, rat tail sign, split fat sign, shape, layer, vascularity, and age, from the 14 candidate variables. The corresponding B coefficient, odds ratio, and p-value of each predictor are presented in Table III. The predictive nomogram that combined all 7 predictors is illustrated in figure 2. The nomogram assigns a score to each variable, reflecting its impact on the outcome event. The total score is calculated based on the patient's specific circumstances and correlates with the probability of predicting schwannomas (fig 3, fig 4).

Performance and validation of the nomogram

When pathological diagnosis was used as the gold standard, the nomogram showed good discrimination for schwannomas, with an AUC of 0.934 (95% confidence interval [CI]: 0.902–0.966) (fig 5a). The calibration curve for the probability of schwannomas demonstrated good concordance between the predicted risk and pathological results (fig 5b). The DCA results demonstrated the potential clinical usefulness and additional value of our predictive model in guiding treatment decisions for patients with schwannoma (fig 5c). To further evaluate the predictive ability of this model without overfitting,

the corrected AUC obtained by internal validation using 10-fold cross-validation with 1000 iterations was 0.921 (95% CI: 0.917-0.924).

Discussion

The further integration of imaging data with additional clinical information is crucial for clinicians in evaluating patient conditions and making surgical decisions [19]. A highly effective approach to achieve this integration is through the application of medical nomograms. These nomograms utilize both biological and clinical variables to formulate a statistical prognostic model that predicts the likelihood of a clinical event for an individual [20]. Both objective variables, such as age, and subjective variables, such as tumor morphology observed in US images, can be concurrently utilized to construct a nomogram [21,22]. In our study, we developed a nomogram based on clinical and US characteristics to provide physicians with a quantitative and visual tool for predicting schwannomas in soft tissue. Our findings revealed that this nomogram facilitated the diagnosis of schwannomas.

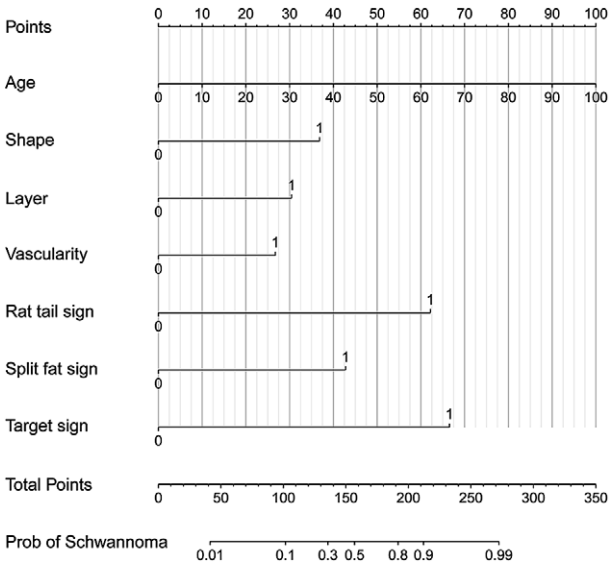

Fig 2. Nomogram to predict the probability of schwannoma. Shape (Regular = 1; Irregular = 0); Layer (Deep = 1; Superficial = 0); Vascularity (Hypervascular = 1; Hypovascular = 0); Rat tail sign (Present = 1; Absent = 0); Split fat sign (Present = 1; Absent = 0); Target sign (Present = 1; Absent = 0).

Table I. The histological types and composition of non-schwannoma lesions

Non-schwannoma lesions	Number (%)	Non-schwannoma lesions	Number (%)
Benign	207 (93.7)	Malignant	14 (6.3)
Hemangioma	42 (19.0)	Fibrosarcoma	4 (1.8)
Lipoma	32 (14.5)	Undifferentiated pleomorphic sarcoma	3 (1.4)
Epidermoid cyst	29 (13.1)	Liposarcoma	2 (0.9)
Neurofibroma	23 (10.4)	Extraskeletal myxoid chondrosarcoma	1 (0.5)
Pilomatrixoma	19 (8.6)	Dermatofibrosarcoma protuberans	1 (0.5)
Giant cell tumor of tendon sheath	16 (7.2)	Malignant granular cell tumor	1 (0.5)
Hidradenoma	7 (3.2)	Esophageal cancer cervical metastasis	1 (0.5)
Ganglion cyst	5 (2.3)	Malignant transformation of neurofibroma	1 (0.5)
Nodular fasciitis	5 (2.3)		
Fibroma	5 (2.3)		
Endometriosis	4 (1.8)		
Desmoid fibromatosis	3 (1.4)		
Inflammatory granuloma	3 (1.4)		
Angioleiomyoma	2 (0.9)		
Trichilemmal cyst	2 (0.9)		
Hamartoma	1 (0.5)		
Giant cell tumor of bone	1 (0.5)		
Carotid body tumor	1 (0.5)		
Lymphangioma	1 (0.5)		
Trichoepithelioma	1 (0.5)		
Leiomyoma	1 (0.5)		
Soft tissue chondroma	1 (0.5)		
Granular cell tumor	1 (0.5)		
Hemangiopericytoma	1 (0.5)		
Proliferative myositis	1 (0.5)		

Table II. Clinical and ultrasound characteristics of patients with schwannomas and non-schwannoma lesions

Characteristics	Schwannomas (n = 80)	Non-schwannoma lesions (n = 221)	T/Z/χ^2	p value
Age, years, mean±SD	51.06±16.16	40.55±18.36	4.525	**<0.001**
Gender – male	46 (57.5%)	114 (51.6%)	0.826	0.364
LMD, cm, Median (Q1, Q3)	2.22 (1.71, 3.18)	2.28 (1.55, 3.45)	-0.020	0.984
SMD, cm, Median (Q1, Q3)	1.28 (0.94, 1.68)	0.96 (0.62, 1.43)	-3.509	**<0.001**
L/S ratio, Median (Q1, Q3)	1.76 (1.51, 2.13)	2.29 (1.73, 3.14)	-4.943	**<0.001**
Location			5.399	0.067
Head and neck	14 (17.5%)	55 (24.9%)		
Trunk	12 (15.0%)	50 (22.6%)		
Limbs	54 (67.5%)	116 (52.5%)		
Layer – superficial	13 (16.3%)	154 (69.7%)	67.897	**<0.001**
Shape – regular	63 (78.7%)	86 (38.9%)	37.288	**<0.001**
Margin – well-defined	78 (97.5%)	160 (72.4%)	22.364	**<0.001**
Rat tail sign – present	47 (58.7%)	16 (7.2%)	94.171	**<0.001**
Target sign – present	34 (42.5%)	7 (3.2%)	77.232	**<0.001**
Split fat sign – present	22 (27.5%)	8 (3.6%)	37.328	**<0.001**
Vessel accompanying sign – present	30 (37.5%)	16 (7.2%)	41.543	**<0.001**
Cystic component – yes	16 (20.0%)	57 (25.8%)	1.073	0.300
Calcification – yes	3 (3.8%)	35 (15.8%)	7.780	**0.005**
Posterior echo enhancement – yes	74 (92.5%)	153 (69.2%)	17.154	**<0.001**
Vascularity – hypervascular	54 (67.5%)	98 (44.3%)	12.599	**<0.001**
Tinel's sign – positive	23 (28.7%)	5 (2.3%)	48.844	**<0.001**

LMD, longitudinal maximum diameter; SMD, short maximum diameter

Moreover, it demonstrated satisfactory performance, as evidenced by a favorable AUC and robust calibration results.

Our findings indicate that target sign, rat tail sign, split fat sign, shape, layer, vascularity, and age are independent predictors of schwannomas, as demonstrated by both univariate and multivariate analyses. Notably, among these predictors, the target sign emerged as the most significant contributor to our nomogram scores, surpassing the rat tail sign. Our previous research demonstrated that the US target sign is a prominent diagnostic feature of schwannomas. Moreover, a good agreement was observed between the target signs detected on US and those identified on MRI [7]. Although the target sign was initially thought to be pathognomonic of neurofibromas, recent MRI studies have revealed that this sign is more common and distinctly defined in schwannomas than in neurofibromas [23,24]. Numerous studies have suggested that the formation of the target sign is closely associated with the distinctive histological composition

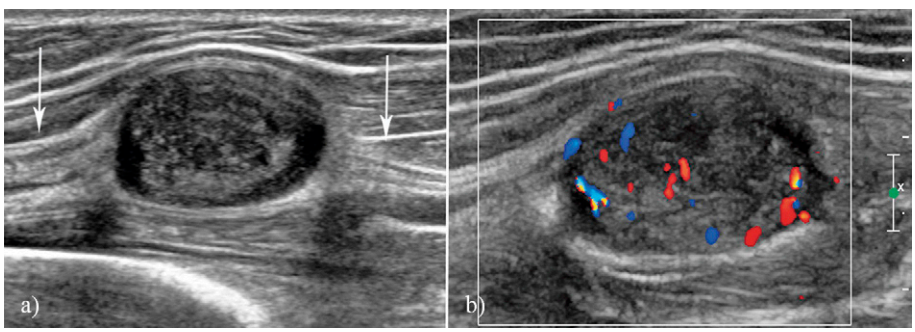

Fig 3. Images from a 40-year-old woman with intermuscular schwannoma in the right upper arm: a) Longitudinal sonogram shows a tumor with a regular shape, affected nerves (arrows) visible at both ends resembling the "rat tail" sign, and a target-like hyperechoic area within the tumor indicating the target sign; b) Color Doppler imaging shows abundant blood flow signals within the tumor. The nomogram assigns a score of 262, indicating a 98.5% probability of schwannoma.

of schwannomas. Specifically, the hyperechoic central region corresponds to the Antoni A area, characterized by a hypercellular component with abundant capillaries and spindle cells displaying nuclear palisading. In contrast, the peripheral hypoechoic region aligns with the Antoni B area, which consists of a hypocellular component with edematous or myxomatous stroma [25,26]. However, recent investigations have revealed novel immunohistochemical findings in schwannomas that demonstrate the MRI target sign. These findings suggest that the central areas contain truly neoplastic cells, while the peripheral regions likely represent mucinous degeneration of the epineurium or perineurium [27].

In this study, the rat tail sign demonstrated a higher detection rate of 58.7% (47/80) compared to 42.5% (34/80) for the target sign; however, it exhibited slightly lower specificity, with values of 92.8% (205/221) versus 96.8% (214/221). Typically, the rat tail sign is considered direct evidence of tumor neurogenicity. However, we found that certain non-neurogenic tumors can also exhibit US characteristics resembling the rat tail sign in non-schwannoma lesions. Noteworthy examples include nodular fasciitis and hemangiopericytoma, which originate from deep fascia and blood vessels, respectively. These tumors extend along the deep fascia or vascular structures at one or both ends, resulting in a US appearance similar to the rat tail sign.

The split fat sign represents a rim of fat encircling a tumor situated within a muscle, most prominently observed at the proximal and distal portions of the nerve [28]. This phenomenon occurs due to the remodeling of fat around the neuromuscular bundle as the tumor gradually enlarges [29]. Although this sign may occasionally appear in other intramuscular soft tissue tumors, it is regarded as one of the most helpful imaging features supporting the diagnosis of intramuscular schwannoma [30]. In contrast, the typical rat tail sign is often difficult to visualize on imaging for intramuscular schwannomas, which typically originate from small nerve branches. However, US can clearly demonstrate the characteristic proliferation of peritumoral adipose tissue.

Most schwannomas are typically located deep within soft tissues, where major nerve trunks traverse intermuscular or intramuscular layers. Although approximately 5% of schwannomas exhibit a plexiform growth pattern characterized by irregular shapes due to the absence of a capsule [3,31], conventional schwannomas are among the few truly encapsulated neoplasms [2], typically displaying regular shapes that appear round or oval. Yuan et al [16] suggest that this regular shape is the most sensitive indicator for evaluating schwannomas. Furthermore, hypervascularization is frequently observed in schwannomas and is correlated with the expression of vascular endothelial growth factor by neoplastic cells. This mechanism provides the theoretical basis for using antiangiogenic therapy with Bevacizumab in the treatment of progressive vestibular schwannomas [31–33].

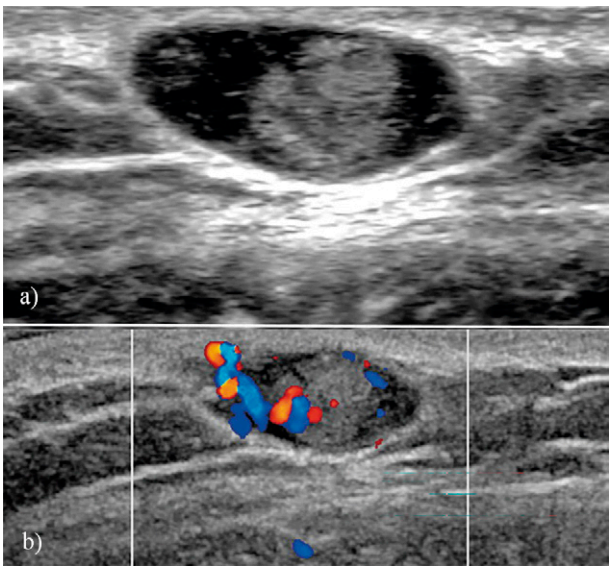

Fig 4. Longitudinal sonograms of a schwannoma in the dermis of the right lower abdominal wall in a 40-year-old man. The tumor displays a regular shape, demonstrates the characteristic target sign (a), and presents with significant blood flow signals (b). The nomogram score for this tumor is 170, suggesting a schwannoma probability of over 60%.

Table III. Predictive factors of schwannoma according to the multivariate logistic regression model

Characteristics	B	Odds ratio (95% CI)	p value
Age	0.040	1.041 (1.015-1.067)	**0.002**
Vascularity	1.064	2.899 (1.250-6.724)	**0.013**
Layer	1.212	3.360 (1.359-8.308)	**0.009**
Shape	1.467	4.335 (1.845-10.189)	**<0.001**
Split fat sign	1.703	5.491 (1.492-20.204)	**0.010**
Rat tail sign	2.475	11.885 (4.519-31.260)	**<0.001**
Target sign	2.648	14.125 (3.849-51.835)	**<0.001**

Surprisingly, age, rather than Tinel's sign, emerged as the sole clinical factor retained in the final predictive model. To facilitate clinical practice, we defined age as a continuous variable in this analysis. Although neurofibromatosis type 2 (NF2)-related schwannomas can occur in patients younger than 30 years, conventional schwannomas predominantly manifest in individuals aged 40–60 years [3,32]. Our findings further support this trend, indicating that schwannomas primarily affect middle-aged and older adults, with an average patient age of 51.06 years, consistent with previous reports [34]. While Tinel's sign demonstrated a significant difference in uni-

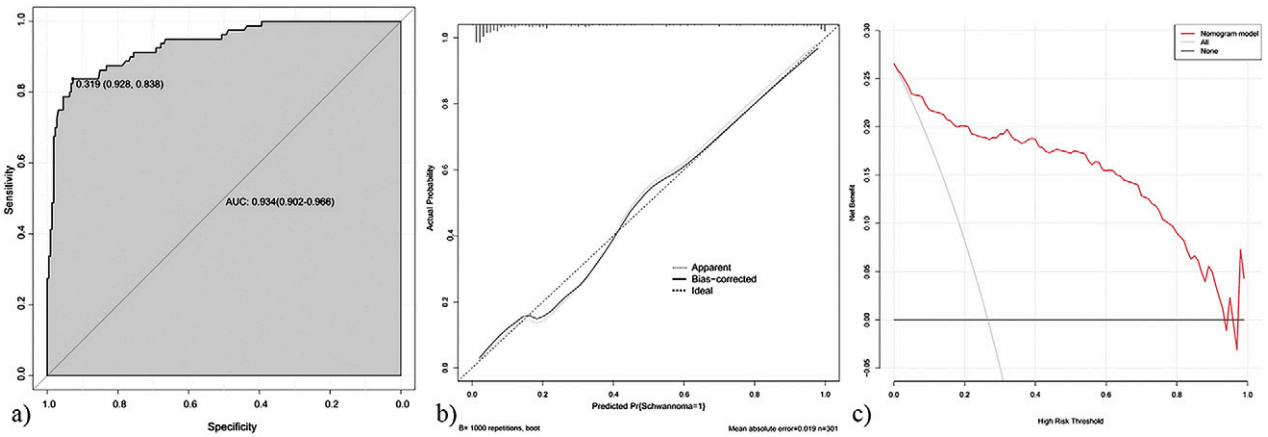

Fig 5. a) The receiver operating characteristic (ROC) curve analysis of the predictive model for schwannoma yields an AUC value of 0.934 (95% CI: 0.902–0.966); b) The calibration curve demonstrates the high predictive ability of our model. The ideal line indicates when predicted and actual probabilities are equal, the apparent line reflects the true predictive scenario for the entire cohort, and the bias-corrected line shows the model's bias correction after 1000 iterations of bootstrap sampling; c) Decision curve analysis (DCA) evaluates clinical utility by calculating net benefit using a probabilistic threshold. The grey line assumes all lesions to be schwannoma (all scheme), while the black line assumes all lesions to be non-schwannoma (none scheme). The red line represents the nomogram model. Our predictive model outperforms both the 'treat-all' and 'treat-none' strategies across a broad range of risk thresholds (0.01–0.93), offering greater overall benefit.

variate analysis, it was ultimately excluded from the final model, possibly due to sample size limitations that may have introduced bias.

However, the results should be interpreted with consideration of the following limitations. First, the patient data were obtained from a single institution; therefore, external validation through multicenter studies is required to confirm the model's generalizability. Second, as a retrospective study, it was subject to selection bias, as only patients with pathological results were included. Third, due to the limited sample size, a separate validation cohort was not established. Nevertheless, internal validation was conducted using a 10-fold cross-validation with 1000 iterations to address this limitation. Fourth, although our study did not assess the model's predictive accuracy for schwannomas in different anatomical locations or layers, we hypothesize that its performance may be less effective for superficial schwannomas compared to deep ones. This limitation likely stems from the fact that subcutaneous schwannomas more frequently exhibit a plexiform growth pattern [6], lack the characteristic split fat sign, and often present challenges in visualizing the rat tail sign. Finally, while the current analysis was limited to conventional US features, future iterations of this model could be improved by incorporating multimodal US parameters such as elastography and contrast-enhanced US characteristics.

In **conclusion**, we have developed a non-invasive predictive model that integrates clinical and US characteristics into a nomogram. This method facilitates the prediction of schwannomas in soft tissue and demonstrates satisfactory performance, thereby providing clinicians with a reliable tool for improving the diagnosis and management of these lesions.

Acknowledgment: This work was supported by the Natural Science Foundation of Nanping, China (N2023J028).

Conflict of interest: none

References

1. Kransdorf MJ. Benign soft-tissue tumors in a large referral population: Distribution of specific diagnoses by age, sex, and location. AJR Am J Roentgenol 1995;164:395–402.
2. Goldblum JR, Lamps LW, McKenney JK, Myers JL, Ackerman LV. Rosai and Ackerman's surgical pathology. 11th ed. Philadelphia, PA: Elsevier; 2018.
3. Moran CA, Kalhoor N, Weissferdt A. (Eds.). Oncological surgical pathology. Cham: Springer International Publishing AG; 2020.
4. Fischerova D, Santos G, Wong L, et al. Imaging in gynecological disease (26): Clinical and ultrasound characteristics of benign retroperitoneal pelvic peripheral-nerve-sheath tumors. Ultrasound Obstet Gynecol 2023;62:727–738.
5. King AD, Ahuja AT, King W, Metreweli C. Sonography of peripheral nerve tumors of the neck. AJR Am J Roentgenol 1997;169:1695–1698.
6. Weidner N, Suster S, Cote RJ, Weiss LM. (Eds.). Modern surgical pathology. 2nd ed. Philadelphia, PA: Saunders/Elsevier; 2009.
7. Yang F, Chen XX, Wu HL, et al. Sonographic features and diagnosis of peripheral schwannomas. J Clin Ultrasound 2017;45:127–133.

8. Levi AD, Ross AL, Cuartas E, Qadir R, Temple HT. The surgical management of symptomatic peripheral nerve sheath tumors. Neurosurgery 2010;66:833–840.
9. Jin Z, Wang C, Wang D, Li X, Guo W, Chen T. Malignant and benign peripheral nerve sheath tumors in a single center: Value of clinical and ultrasound features for the diagnosis of malignant peripheral nerve sheath tumor compared with magnetic resonance imaging. J Ultrasound Med 2024;43:21–31.
10. Wu WT, Mezian K, Naňka O, et al. Enhancing diagnosis and treatment of superior cluneal nerve entrapment: Cadaveric, clinical, and ultrasonographic insights. Insights Imaging 2023;14:116.
11. Lin TY, Chang KV, Wu WT, Özçakar L. Ultrasonography for the diagnosis of carpal tunnel syndrome: an umbrella review. J Neurol 2022;269:4663–4675.
12. Gosk J, Gutkowska O, Urban M, Martynkiewicz J, Bąk M, Ziółkowski P. Benign nerve tumours of the hand (excluding wrist). Arch Orthop Trauma Surg 2015;135:1763–1769.
13. Irwin RW, Wolff ET. Assessment of neuromuscular conditions using ultrasound. Phys Med Rehabil Clin N Am 2014;25:531–543.
14. Gruber H, Glodny B, Bendix N, Tzankov A, Peer S. High-resolution ultrasound of peripheral neurogenic tumors. Eur Radiol 2007;17:2880–2888.
15. Aparisi Gómez MP, Errani C, Lalam R, et al. The role of ultrasound in the diagnosis of soft tissue tumors. Semin Musculoskelet Radiol 2020;24:135–155.
16. Yuan Y, Gao J, Xiong G, Guo L. Diagnostic accuracy of multiparametric ultrasound for peripheral nerve schwannoma. Acta Radiol 2023;64:1608–1614.
17. Ogata D, Takeji M, Murakami T, Yanagisawa H, Kuramochi A, Tsuchida T. Comparison of ultrasonographic findings of schwannomas and angioleiomyomas. J Dermatol 2018;45:837–843.
18. Adler DD, Carson PL, Rubin JM, Quinn-Reid D. Doppler ultrasound color flow imaging in the study of breast cancer: Preliminary findings. Ultrasound Med Biol 1990;16:553–559.
19. Sun P, Han J, Li M, et al. Spectral ultrasound combined with clinical pathological parameters in prediction of axillary lymph node metastasis in breast cancer. J Ultrasound Med 2024;43:2311–2324.
20. Balachandran VP, Gonen M, Smith JJ, DeMatteo RP. Nomograms in oncology: More than meets the eye. Lancet Oncol 2015;16:e173–e180.
21. Lei Z, Li J, Wu D, et al. Nomogram for preoperative estimation of microvascular invasion risk in hepatitis B virus–related hepatocellular carcinoma within the milan criteria. JAMA Surg 2016;151:356–363.
22. Wang H, Lai J, Li J, et al. Does establishing a preoperative nomogram including ultrasonographic findings help predict the likelihood of malignancy in patients with microcalcifications? Cancer Imaging 2019;19:46.
23. Ahlawat S, Fayad LM. Imaging cellularity in benign and malignant peripheral nerve sheath tumors: Utility of the "target sign" by diffusion weighted imaging. Eur J Radiol 2018;102:195–201.
24. Shirodkar K, Hussein M, Reddy PS, et al. Imaging of peripheral intraneural tumors: A comprehensive review for radiologists. Cancers 2025;17:246.
25. Koga H, Matsumoto S, Manabe J, Tanizawa T, Kawaguchi N. Definition of the target sign and its use for the diagnosis of schwannomas. Clin Orthop Relat Res 2007;464:224–229.
26. Wu W, Ding Y, Su Y, et al. Novel MRI signs for differentiating neurogenic and non-neurogenic peripheral nerve tumors: Insights from contrast-enhanced magnetic resonance neurography. Eur J Radiol 2025;183:111894.
27. Ishizawa M, Okabe H, Matsumoto K, Morimoto S, Hukuda S, Chano T. Histopathological explanation of the MRI target sign in extra-axial schwannomas. J Orthop Sci 2021;26:660–665.
28. Crist J, Hodge JR, Frick M, et al. Magnetic resonance imaging appearance of schwannomas from head to toe: A pictorial review. J Clin Imaging Sci 2017;7:38.
29. Deka JB, Shah R, Jiménez M, et al. A retrospective analysis of high resolution ultrasound evaluation of the "split fat sign" in peripheral nerve sheath tumors. Healthcare (Basel) 2023;11:3147.
30. Salunke AA, Chen Y, Tan JH, et al. Intramuscular schwannoma: Clinical and magnetic resonance imaging features. Singapore Med J 2015;56:555–557.
31. Belakhoua SM, Rodriguez FJ. Diagnostic pathology of tumors of peripheral nerve. Neurosurgery 2021;88:443–456.
32. Kloth C, Eissler A, Schmidberger J, et al. Quantitative analysis of superb microvascular imaging versus color-coded doppler sonography for preoperative evaluation of vascularization of schwannomas. J Neurol Surg A Cent Eur Neurosurg 2020;81:213–219.
33. Plotkin SR, Duda DG, Muzikansky A, et al. Multicenter, prospective, phase II and biomarker study of high-dose bevacizumab as induction therapy in patients with neurofibromatosis type 2 and progressive vestibular schwannoma. J Clin Oncol 2019;37:3446–3454.
34. Ryu JA, Lee SH, Cha EY, Kim TY, Kim SM, Shin MJ. Sonographic differentiation between schwannomas and neurofibromas in the musculoskeletal system. J Ultrasound Med 2015;34:2253–2260.